

## First Detection of Radio Linear Polarization of GRB Afterglow

YUJI URATA,<sup>1</sup> KENJI TOMA,<sup>2,3</sup> KUIYUN HUANG,<sup>4</sup> KEIICHI ASADA,<sup>5</sup> HIROSHI NAGAI,<sup>6,7</sup> SATOKO TAKAHASHI,<sup>8,9,7</sup>  
GLEN PETITPAS,<sup>10</sup> MAKOTO TASHIRO,<sup>11</sup> AND KAZUTAKA YAMAOKA<sup>12,13</sup>

<sup>1</sup>*Institute of Astronomy, National Central University, Chung-Li 32054, Taiwan*

<sup>2</sup>*Frontier Research Institute for Interdisciplinary Sciences, Tohoku University, Sendai 980-8578, Japan*

<sup>3</sup>*Astronomical Institute, Tohoku University, Sendai, 980- 8578, Japan*

<sup>4</sup>*Center for General Education, Chung Yuan Christian University, Taoyuan 32023, Taiwan*

<sup>5</sup>*Academia Sinica Institute of Astronomy and Astrophysics, Taipei 106, Taiwan*

<sup>6</sup>*National Astronomical Observatory of Japan, 2-21-1 Osawa, Mitaka Tokyo 181-8588, Japan*

<sup>7</sup>*Department of Astronomical Science, School of Physical Sciences, SOKENDAI (The Graduate University for Advanced Studies), Mitaka, Tokyo 181-8588, Japan*

<sup>8</sup>*Joint ALMA Observatory, Alonso de Cordova 3108, Vitacura, Santiago, Chile*

<sup>9</sup>*NAOJ Chile Observatory, Alonso de Crdova 3788, Oficina 61B, Vitacura, Santiago, Chile*

<sup>10</sup>*Harvard-Smithsonian Center for Astrophysics, 60 Garden Street, Cambridge, Massachusetts 02138, USA*

<sup>11</sup>*Department of Physics, Saitama University, Shimo-Okubo, Saitama, 338-8570, Japan*

<sup>12</sup>*Institute for Space-Earth Environmental Research (ISEE), Nagoya University, Furo-cho, Chikusa-ku, Nagoya, Aichi 464- 8601, Japan*

<sup>13</sup>*Division of Particle and Astrophysical Science, Graduate School of Science, Nagoya University, Furo-cho, Chikusa-ku, Nagoya, Aichi 464-8601, Japan*

Submitted to ApJL

### ABSTRACT

We report the first detection of radio polarization of a GRB afterglow with the first intensive combined use of telescopes in the millimeter and submillimeter ranges for GRB171205A. The linear polarization degree in the millimeter band at the sub-percent level ( $0.27 \pm 0.03\%$ ) is lower than those observed in late-time optical afterglows (weighted average of  $\sim 1\%$ ). The Faraday depolarization by non-accelerated, cool electrons in the shocked region is one of the most likely mechanisms for the low value. In this scenario, larger total energy by a factor of  $\sim 10$  than ordinary estimate without considering non-accelerated electrons is required. The variation of the position angle along with wavelength is not inconsistent with this scenario. This result indicates that polarimetry in the millimeter and submillimeter ranges is a unique tool for investigating GRB energetics, and coincident observations with multiple frequencies or bands would provide more accurate measurements of the non-accelerated electron fraction.

*Keywords:* acceleration of particles, polarization, (stars:) gamma-ray burst: individual (GRB171205A)

### 1. INTRODUCTION

Gamma-ray Bursts (GRBs) are highly energetic explosions in the universe, and are currently being exploited as probes of first-generation stars and gravitational wave transients. In fact, the distant events at the re-ionization epoch (Tanvir et al. 2009; Cucchiara et al. 2011; Totani et al. 2014) and the short GRB coincident

with a gravitational wave transient have already been observed (Abbott et al. 2017), respectively. The energetics of GRBs are fundamental physical parameters that can not only reveal their progenitor systems but also probe both the early and current states of the universe. Although substantial observational efforts have been made since the afterglow discovery (Costa et al. 1997), the total energies have been estimated so far without considering non-accelerated, cool electrons at the relativistic collisionless shocks that do not emit observable radiation (Eichler & Waxman 2005), while the

existence of such cool electrons is well studied for supernova remnants and solar winds (e.g. [van Adelsberg et al. 2008](#); [Vink et al. 2015](#)). A clear method for identifying non-accelerated electrons in GRB afterglows is measurement of their Faraday effect that suppresses the radio polarization but keeps the optical one as emitted ([Toma et al. 2008](#))<sup>1</sup>. Here, we report the first detection of radio polarization of a GRB afterglow through observing low-luminosity GRB 171205A, and discuss implications from the Faraday depolarization model.

GRB 171205A was detected on 5 December 2017, 07:20:43 UT ([D’Elia et al. 2017](#)) and its X-ray and optical afterglows ([D’Elia et al. 2018](#)) are identified by the Neil Gehrels Swift Observatory. [Izzo et al. \(2017\)](#) made spectroscopic observations with the Very Large Telescope (VLT) in Chile approximately 1.5 h after the GRB by identifying the optical afterglow and, based on the absorption and emission lines, announced a redshift of  $z = 0.0368$ . At this redshift, the isotropic  $\gamma$ -ray energy release  $E_{\gamma, \text{iso}}$  of  $2.4 \times 10^{49}$  erg (in the 20–1500 keV range with the cosmological parameters  $H_0 = 70 \text{ km s}^{-1} \text{ Mpc}^{-1}$ ,  $\Omega_m = 0.3$ , and  $\Omega_\Lambda = 0.7$ ) indicates that GRB171205A is categorized as a low-luminosity GRB. Intensive optical photometric and spectroscopic observations using the 10.4-m Gran Telescopio CANARIAS (GTC) revealed the association of a broad-line type Ic supernova that resembled SN1998bw ([de Ugarte Postigo et al. 2017](#)). The bright millimeter afterglow was also detected by the Northern Extended Millimeter Array (NOEMA) in the 90 GHz and 150 GHz bands 20.2 h after the burst ([de Ugarte Postigo et al. 2017](#)).

## 2. OBSERVATIONS AND ANALYSIS

### 2.1. SMA

Intensive monitoring was made using the SMA at 230 GHz starting 6 December 2017 with a total of six epochs. On the nights of 8 and 13 December 2017, the afterglow was observed by the dual-band mode at 230 and 345 GHz. The data were flagged and calibrated with the MIR data-reduction package using standard procedures and were then imaged using Miriad software ([Sault et al. 1995](#)). Except for the observation at 345 GHz on 13 December 2017 (due to marginal weather conditions in the band), the afterglow was clearly detected at a confidence level of more than  $10\sigma$ . Flux measurements were performed using Common Astronomy Software Applications (CASA, ver-

sion 5.1.1; [McMullin et al. 2007](#)). Although the 150-GHz NOEMA observation reported the second brightest GRB in the millimeter band ([de Ugarte Postigo et al. 2017](#)), we measured an unusual bright submillimeter afterglow of  $53.7 \pm 0.9 \text{ mJy}$  in the 230 GHz band 1.5 days after GRB, which is the brightest afterglow in the submillimetre range. At the same epoch, the historical GRB030329 was  $49.2 \pm 1.1 \text{ mJy}$  in the 250 GHz band ([Sheth et al. 2003](#)). Furthermore, the brightness of the GRB171205A afterglow was 510 times brighter than other bright afterglows detected by SMA at 230 GHz ([Urata et al. 2014, 2015](#)), which are expected to be suitable polarimetry targets in the millimetre range with the typical afterglow temporal evolution. Thus, GRB 171205A is an ideal object for performing the first radio polarimetry.

### 2.2. ALMA

ALMA observed the afterglow in two different epochs using the linear polarization mode at Band 3 (representative frequency of 97.5 GHz) on 10 and 16 December 2017. The correlator processed four spectral windows (SPWs) centered at 90.5, 92.5, 102.5, and 104.5 GHz with a bandwidth of 1.75 GHz each. The bandpass and flux were calibrated using observations of J1127-1857, and J1130-1149 was used for the phase calibration. The polarization calibration was performed by observations of J1256-0547. The raw data were reduced at the East Asian ALMA Regional Center (EA-ARC) using CASA (version 5.1.1). We further performed iterative CLEAN deconvolution imaging with self-calibration. The Stokes  $I$ ,  $Q$ , and  $U$  maps were CLEANed with an appropriate number of CLEAN iterations after the final round of self-calibration. Since significant signals were observed on the Stokes  $Q$  and  $U$  maps generated using the entire Band 3 dataset from 10 December 2017, we generated additional Stokes maps using the individual SPWs. The quantities that can be derived from the polarization maps are the polarized intensity, polarization degree, and polarization position angle (P.A.). The *atan2* function in the python math module which returns a numeric value between  $-\pi$  and  $\pi$ , was used to calculate the polarization position angle. The non-detection (both positive and negative) with  $S/N$  of 3 on the 92.5-GHz  $U$  map taken on 10 December 2017 yielded polarization position angle ranges of  $\text{P.A.} > +78^\circ$  and  $\text{P.A.} < -78^\circ$ .

The ACA observations were executed on 10, 12, and 16 December 2017 at 345 GHz (Band 7) with the single continuum observing mode. Two of the ACA photometry observations were conducted during polarimetry using ALMA. The data were flagged, calibrated and

<sup>1</sup> Other methods via spectroscopy of GRB afterglows are discussed in [Ressler & Laskar \(2017\)](#) and [Warren et al. \(2018\)](#).

imaged with standard procedures with CASA (version 5.1.1).

### 2.3. VLA

VLA observed the afterglow on 9 December 2017 at central frequencies of 6 GHz (C-band), 10 GHz (X-band), and 15 GHz (U-band), as one of the observatory-sponsored observations (Laskar et al. 2017). The data were calibrated using standard tools in CASA (VLA pipeline version 5.0.0) and then were imaged with CLEAN task. The source was significantly (more than  $50\sigma$ ) detected in all three bands. To describe the spectral energy distribution, six images at the central frequencies of 5 GHz, 7 GHz, 8.5 GHz, 11 GHz, 13.5 GHz, and 16 GHz were generated with the CLEAN task, and qualified photometry was performed with a confidence level of more than  $20\sigma$ .

## 3. RESULTS

### 3.1. Lightcurve and SED

The temporal evolution of the afterglow flux at 230 GHz is described by broken power-law decays ( $f_\nu(t) \propto t^\alpha$ ) with  $\alpha = -0.30 \pm 0.07$  for  $t \lesssim 4$  days and  $\alpha = -1.34 \pm 0.06$  for  $t \gtrsim 4$  days, as show in Figure 1. The spectral slope ( $f_\nu \propto \nu^\beta$ ) is also described as  $\beta = 1.457 \pm 0.028$  at 4.3 days in the centimeter range (5–16 GHz; Figure 2a) and  $\beta = -0.430 \pm 0.004$  at 5.2 days in the submillimeter and millimeter range (90.5–345 GHz; Figure 2a). High-quality photometry ( $S/N \sim 72$ –89) using ALMA during the polarimetry, at 5.2 days, measured the spectral slope of  $\beta = -0.40 \pm 0.01$  in the 90–100 GHz (i.e. Band 3). These measurements indicate that the spectral peak was located at  $\sim 30$  GHz (below  $\sim 90$  GHz).

### 3.2. Polarization

Figure 3a shows the Stokes  $I$ ,  $Q$ , and  $U$  maps obtained using the entire ALMA Band 3 frequency range taken 5.2 days after the GRB. Detections with a confidence level of  $5\sigma$  or better on the  $Q$  and  $U$  maps yield a polarization degree of  $0.27 \pm 0.03\%$ . Our measured value describes the intrinsic origin because depolarization between the source and observing site is negligible for the point source (i.e. GRB afterglows) in this millimeter band (Brentjens & de Bruyn 2005). Although we could not find any detection in the Stokes  $Q$  and  $U$  maps at 11.2 days, we measured the corresponding deep upper limit of the polarization degree ( $< 0.27\%$ ,  $3\sigma$  significance), which was consistent with that at 5.2 days within the error margin.

The apparent brightness of  $31.94 \pm 0.44$  mJy observed 5.2 days after the burst using the entire ALMA Band 3 frequency range enabled more detailed polarimetric

analysis using four individual spectral windows (SPW) of Band 3 (Figure 3 b, c, d, and e). The measurments are summarized in Table 1. Other than the Stokes  $U$  map at 92.5 GHz, there were significant detections at a  $3.0\sigma$  confidence level or better. In the Stokes  $U$  map at 92.5 GHz, there was no significant flux, and the range of the P.A. was constrained. Although the polarization degrees in each SPW were consistent with the value measured using the entire Band 3 frequency, the P.A. significantly varied with the wavelength (Figure 4). The observed P.A. is most likely intrinsic value because the Faraday rotation effect for both the host galaxy and Milky Way Galaxy is quite small at this frequency (Sokoloff et al. 1998; Oppermann et al. 2012). The expected galactic Faraday rotation effect is up to  $\sim 0.3^\circ$ . We tried to fit the P.A. data including the upper limit (the method is described in Sawicki 2012) with constant or linear function of squared wavelength, but did not obtain a good fit (Figure 4).

## 4. DISCUSSION

### 4.1. Afterglow modeling

The spectral data and the light curve at 230 GHz for 1–10 days can be explained by the standard forward shock model (e.g. Granot & Sari 2002). The closure relation (Zhang & Mészáros 2004) at  $t \gtrsim 4$  days is  $\alpha - 3\beta/2 \simeq -0.69 \pm 0.07$ . The standard synchrotron emission from the forward shock expanding in uniform density medium for  $\nu_m < \nu < \nu_c$  obeys  $\alpha - 3\beta/2 = 0$  when the edge of the collimated shock is not observed due to the relativistic beaming effect. After the edge can be observed (but the shock does not expand sideways), the additional geometrical flux reduction  $\Gamma^2 \theta_j^2 \propto t^{-3/4}$  leads to  $\alpha - 3\beta/2 = -3/4$ , where  $\Gamma$  and  $\theta_j$  are the Lorentz factor and opening half-angle of the shock, respectively. The latter relation is consistent with our observation. The decay index for  $\nu_a < \nu < \nu_m$  in this model is  $\alpha = -1/4$ , which is also consistent with that for  $t \lesssim 4$  days. Therefore, the break in the 230 GHz light curve is due to the  $\nu_m$  crossing.

Based on this model, the spectra at  $t = 4.3$  and 5.2 days and the multiband light curves can be well fitted by the flux formula of Granot & Sari (2002) multiplied by the geometrical flux reduction factor  $[1 + (t/t_j)]^{-3/4}$  (Figure 1, 2a). Here we set the synchrotron self-absorption frequency  $\nu_a \simeq 22$  GHz, the synchrotron frequency of minimum-energy electrons  $\nu_m \simeq 200 (t/4.3 \text{ days})^{-3/2}$  GHz, the peak flux before the jet break  $F_{\nu_m}(t < t_j) \simeq 72$  mJy, the jet break time  $t_j \simeq 2$  days, and the electron energy spectral index  $p \simeq 3$ . The first three characteristic quantities are functions of four physical parameters, namely the isotropic

shock energy  $E_{\text{iso}}$ , the ambient medium density  $n$ , the fraction of shock energy carried by the electrons  $\epsilon_e$ , and that carried by amplified magnetic field  $\epsilon_B$ . Thus, we have the relations  $n \simeq 20 (E_{\text{iso}}/2 \times 10^{50} \text{ erg})^3 \text{ cm}^{-3}$ ,  $\epsilon_e \simeq 0.03 (E_{\text{iso}}/2 \times 10^{50} \text{ erg})$ , and  $\epsilon_B \simeq 0.005 (E_{\text{iso}}/2 \times 10^{50} \text{ erg})^{-5}$ . The numerical values of  $n$ ,  $\epsilon_e$ , and  $\epsilon_B$  are typical of GRB afterglows (Panaitescu & Kumar 2002), and thus,  $E_{\text{iso}}$  may not be considerably different from this value due to the high dependences of  $n$  and  $\epsilon_B$  on  $E_{\text{iso}}$ . This analysis means that we performed the first radio afterglow polarimetry in the waveband well above  $\nu_a$  (c.f. Granot & Taylor 2005; van der Horst et al. 2014).

#### 4.2. Faraday depolarization effect

We focused on the polarization at 5.2 days, the phase when the intensity can be explained by the standard forward shock model. The precise detection of the polarization degree of  $0.27 \pm 0.03\%$  indicated that the value is the smallest one among all afterglow polarization measurements, and smaller than those in late-time optical afterglows explained by the standard forward shock model, which range from 0.5% to 10% (Greiner et al. 2003; Wiersema et al. 2014; Covino & Gotz 2016).

There was no polarimetric data at the higher frequency ranges for the present event (except the supernova component in the optical band). Note that there are 84 polarimetric measurements for optical afterglows (i.e. excluding measurements for early-time reverse shock components that show high values) among 13 GRBs (Covino & Gotz 2016). The weighted average and average of the measurements are 1.0% and 1.6%, respectively. Among these, 58 measurements were made during the phases in which the intensities are describable by the standard forward shock model. For these selected events, the weighted average and average of the linear polarizations are 1.2% and 1.7%, respectively.

By assuming a polarization degree at higher frequency ranges (e.g. optical) for the present event as  $P_0 = 1\%$ , we calculate the polarization spectrum based on the afterglow model described above (c.f. Matsumiya & Ioka 2003; Sagiv et al. 2004; Jones & O'Dell 1977; Huang & Shcherbakov 2011), and plot it by the grey dotted line in Figure 2b. It varies by a factor of  $0.5(p + 7/3)/(p + 1) \simeq 2/3$  at  $\nu = \nu_m$  and decays at  $\nu \lesssim \nu_a$ . Our measured value is substantially lower than this model line.

It has long been theoretically predicted that, if only part of the swept-up electrons is accelerated, the non-accelerated electrons with thermal Lorentz factor  $\tilde{\gamma}_m = \eta\Gamma$  cause Faraday depolarization at  $\nu > \nu_a$  (Toma et al. 2008), where  $\eta$  is a factor of the order of unity in the case that the non-accelerated electrons are just isotropized at the shock front (Eichler & Waxman

2005). Such a model in which the fraction of accelerated electrons is  $f < 1$  can explain the intensity in the same way as in the standard model with the parameters  $E'_{\text{iso}} = E_{\text{iso}}/f$ ,  $n' = n/f$ ,  $\epsilon'_e = \epsilon_e f$ , and  $\epsilon'_B = \epsilon_B f$  (Eichler & Waxman 2005). Thus, a very small value of  $f$  would lead to a crisis of the total energy requirement. In this scenario, the polarization degree is given by  $P_0 \sin(\tilde{\tau}_V/2)/(\tilde{\tau}_V/2)$  where  $\tilde{\tau}_V = (\nu/\tilde{\nu}_V)^{-2}$  and  $\tilde{\nu}_V \sim 200 [(1-f)/10f]^{1/2} \eta^{-1} \sqrt{\ln \tilde{\gamma}_m} N^{-1/12} (E_{\text{iso}}/10^{52} \text{ erg})^{3/16} n^{9/16} (\epsilon_B/0.01)^{1/4} (t/1 \text{ day})^{-1/16} \text{ GHz}$ . Here the magnetic field in the shocked region has been assumed to be tangled on hydrodynamic scales, following Toma et al. (2008) and Uehara et al. (2012), and then the plasma can be considered to consist of a number of random cells, in each of which magnetic field is ordered (Jones & O'Dell 1977; Gruzinov & Waxman 1999).  $N$  denotes the number of random cells in the three-dimensional visible region. In this case  $P_0 = (p + 1)/[(p + 7/3)\sqrt{N}]$  for  $\nu > \nu_m$  while  $P_0 = 0.5/\sqrt{N}$  for  $\nu_a < \nu < \nu_m$ . With  $P_0 = 1\%$  for  $\nu > \nu_m$ ,  $\tilde{\nu}_V \simeq 210 \text{ GHz}$  explains our measurement (see the green dashed line in Figure 2b), which corresponds to  $1/f \sim 12 (E_{\text{iso}}/2 \times 10^{50} \text{ erg})^{-5/4} \eta^2 (\ln \tilde{\gamma}_m)^{-1}$ . For the case of  $P_0 = 0.5\%$  (Figure 2b),  $1/f \sim 10$  is still required.

The P.A. becomes a very complicated function of wavelength and the functional form is determined randomly for such a tangled magnetic field that we assume (Sokoloff et al. 1998). Therefore, the observed variation of the P.A. is not inconsistent with this scenario.

In summary, with the first intensive combined use of telescopes in the millimeter and submillimeter ranges for the GRB171205A afterglow, our observations provided the first linear polarimetry in the millimeter band. The measured polarization degree is substantially lower than the typical optical one. Although the (semi-) simultaneous measurements in multiple wavelengths are required, this measurement suggests the Faraday depolarization effect and larger total energy by a factor of  $\sim 10$  than ordinary estimate without considering non-accelerated electrons. The observed P.A. variation along with wavelength is not inconsistent with this scenario. Multi-frequency polarimetry in the submillimeter/millimeter range and/or with simultaneous optical polarimetry would provide more accurate non-accelerated electron fraction. Hence, this observation consolidates the new methodology for revealing the fundamental properties of GRBs.

This paper makes use of the following ALMA data: ADS/JAO.ALMA#2017.1.00801.T. ALMA is a partnership of ESO (representing its member states),



NSF (USA), and NINS (Japan), together with NRC (Canada), MOST and ASIAA (Taiwan), and KASI (Republic of Korea), in cooperation with the Republic of Chile. The Joint ALMA Observatory is operated by ESO, AUI/NRAO, and NAOJ. This work is supported by the Ministry of Science and Technology of Taiwan grants MOST 105-2112-M-008-013-MY3 (Y.U.) and 106-2119-M-001-027 (K.A.). This work is also supported by JSPS Grants-in-Aid for Scientific Research

No. 18H01245 (K.T.). We thank EA-ARC, especially Pei-Ying Hsieh for support in the ALMA observations. We also thank P. T. P. Ho and Y. Ohira for helpful comments. Y.U., K. Y. H., and K. A. also thank Ministry of Education Republic of China.

*Facilities:* ALMA, SMA, VLA

*Software:* CASA (McMullin et al. 2007),

## REFERENCES

- Abbott, B. P., Abbott, R., Abbott, T. D., et al. 2017, *ApJL*, 848, L13
- Brentjens, M. A., & de Bruyn, A. G. 2005, *A&A*, 441, 1217
- Costa, E., Frontera, F., Heise, J., et al. 1997, *Nature*, 387, 783
- Covino, S., & Gotz, D. 2016, *Astronomical and Astrophysical Transactions*, 29, 205
- Cucchiara, A., Levan, A. J., Fox, D. B., et al. 2011, *ApJ*, 736, 7
- D’Elia, V., D’Ai, A., Lien, A. Y., & Sbarufatti, B. 2017, *GRB Coordinates Network, Circular Service*, No. 22177, #1 (2017), 22177, 1
- D’Elia, V., Campana, S., D’Ai, A., et al. 2018, *A&A*, 619, A66
- de Ugarte Postigo, A., Izzo, L., Kann, D. A., et al. 2017, *GRB Coordinates Network, Circular Service*, No. 22204, #1 (2017), 22204, 1
- de Ugarte Postigo, A., Schulze, S., Bremer, M., et al. 2017, *GRB Coordinates Network, Circular Service*, No. 22187, #1 (2017), 22187, 1
- Eichler, D., & Waxman, E. 2005, *ApJ*, 627, 861
- Granot, J., & Sari, R. 2002, *ApJ*, 568, 820
- Granot, J., & Taylor, G. B. 2005, *ApJ*, 625, 263
- Greiner, J., Klose, S., Reinsch, K., et al. 2003, *Nature*, 426, 157
- Gruzinov, A., & Waxman, E. 1999, *ApJ*, 511, 852
- Huang, L. & Shcherbakov, R. V. 2011, *MNRAS*, 416, 2574
- Izzo, L., Selsing, J., Japelj, J., et al. 2017, *GRB Coordinates Network, Circular Service*, No. 22180, #1 (2017), 22180, 1
- Jones, T. W., & O’Dell, S. L. 1977, *ApJ*, 214, 522
- Laskar, T., Coppejans, D. L., Margutti, R., & Alexander, K. D. 2017, *GRB Coordinates Network, Circular Service*, No. 22216, #1 (2017), 22216, 1
- Matsumiya, M., & Ioka, K. 2003, *ApJ*, 595, L25
- McMullin, J. P., Waters, B., Schiebel, D., Young, W., & Golap, K. 2007, *Astronomical Data Analysis Software and Systems XVI*, 376, 127
- Oppermann, N., Junklewitz, H., Robbers, G., et al. 2012, *A&A*, 542, A93
- Panaitescu, A., & Kumar, P. 2002, *ApJ*, 571, 779
- Ressler, S. M., & Laskar, T. 2017, *ApJ*, 845, 150
- Sagiv, A., Waxman, E., & Loeb, A. 2004, *ApJ*, 615, 366
- Sault, R. J., Teuben, P. J., & Wright, M. C. H. 1995, *Astronomical Data Analysis Software and Systems IV*, 77, 433
- Sawicki, M. 2012, *PASP*, 124, 1208
- Sheth, K., Frail, D. A., White, S., et al. 2003, *ApJL*, 595, L33
- Sokoloff, D. D., Bykov, A. A., Shukurov, A., et al. 1998, *MNRAS*, 299, 189
- Tanvir, N. R., Fox, D. B., Levan, A. J., et al. 2009, *Nature*, 461, 1254
- Toma, K., Ioka, K., & Nakamura, T. 2008, *ApJL*, 673, L123
- Totani, T., Aoki, K., Hattori, T., et al. 2014, *PASJ*, 66, 63
- Uehara, T. et al. 2012, *ApJ*, 752, L6
- Urata, Y., Huang, K., Takahashi, S., et al. 2014, *ApJ*, 789, 146
- Urata, Y., Huang, K., Asada, K., et al. 2015, *Advances in Astronomy*, 2015, 165030
- van Adelsberg, M., Heng, K., McCray, R., & Raymond, J. C. 2008, *ApJ*, 689, 1089
- van der Horst, A. J., Paragi, Z., de Bruyn, A. G., et al. 2014, *MNRAS*, 444, 3151
- Vink, J., Broersen, S., Bykov, A., & Gabici, S. 2015, *A&A*, 579, A13
- Warren, D. C., Barkov, M. V., Ito, H., Nagataki, S., & Laskar, T. 2018, *MNRAS*, 480, 4060
- Wiersema, K., Covino, S., Toma, K., et al. 2014, *Nature*, 509, 201
- Zhang, B., & Mészáros, P. 2004, *International Journal of Modern Physics A*, 19, 2385

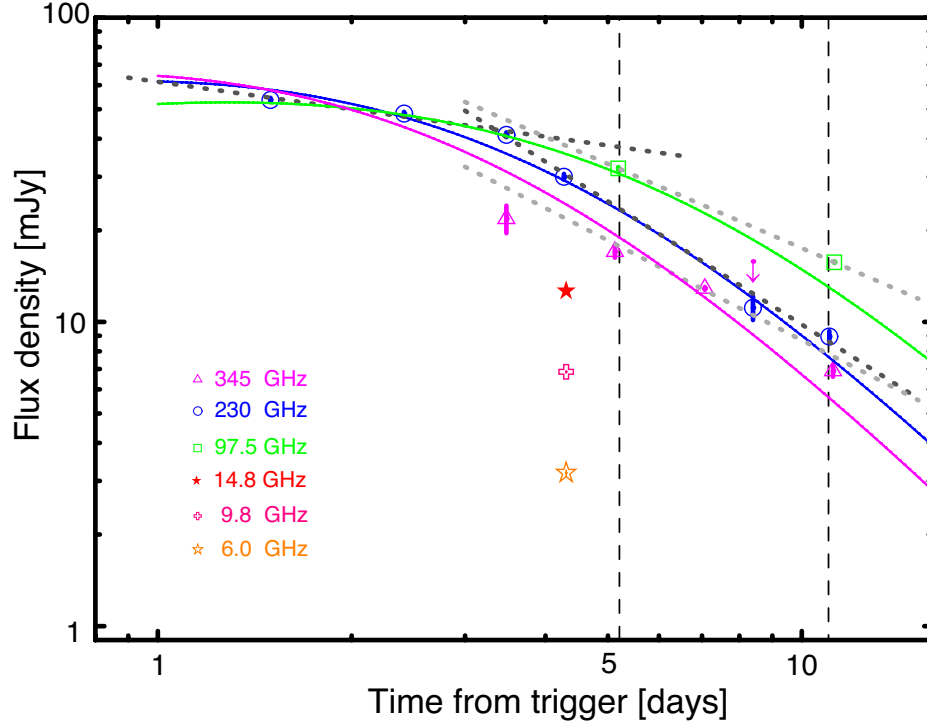


**Figure 1.** Radio afterglow light curves. Solid lines indicate the model light curves at 97.5 GHz (green), 230 GHz (blue), and 345 GHz (magenta) based on the standard forward shock model. Dark grey dotted lines show the simple power-law fittings for 230 GHz data before and 4 days after the burst. Light grey dotted lines show the simple power-law fitting for 97.5 GHz and 345 GHz data after 4 days. Light grey dashed lines indicate the epochs of ALMA polarimetry.

**Table 1.** ALMA Band 3 Polarization Observing Log

| Epoch1: 2017-12-10 10:23-13:17, T=5.187 days  |            |                   |                              |                    |                    |                    |
|---|------------|-------------------|------------------------------|--------------------|--------------------|--------------------|
| SPW   | Band [GHz] | Pol. [%]          | P.A [deg]                    | I flux [mJy]       | Q flux [mJy]       | U flux [mJy]       |
| 0,1,2,3                                       | 97.5       | $0.272 \pm 0.032$ | $-71.3 \pm 3.3$              | $31.944 \pm 0.440$ | $-0.069 \pm 0.009$ | $-0.053 \pm 0.011$ |
| 0   | 90.5       | $0.300 \pm 0.050$ | $-67.9 \pm 4.7$              | $32.719 \pm 0.413$ | $-0.070 \pm 0.010$ | $-0.069 \pm 0.020$ |
| 1   | 92.4       | $< 0.316$         | $< -78.1 \text{ or } > 78.1$ | $32.514 \pm 0.365$ | $-0.094 \pm 0.026$ | 0.014(rms)         |
| 2   | 102.5      | $0.348 \pm 0.066$ | $-71.3 \pm 5.5$              | $31.172 \pm 0.399$ | $-0.086 \pm 0.025$ | $-0.066 \pm 0.018$ |
| 3   | 104.5      | $0.314 \pm 0.054$ | $-58.0 \pm 4.9$              | $30.898 \pm 0.412$ | $-0.043 \pm 0.012$ | $-0.087 \pm 0.029$ |
| Epoch2: 2017-12-16 11:14-14:33, T=11.231 days |            |                   |                              |                    |                    |                    |
| SPW   | Band [GHz] | Pol. [%]          | P.A [deg]                    | I flux [mJy]       | Q flux [mJy]       | U flux [mJy]       |
| All   | 97.5       | $< 0.267$         | —                            | $15.705 \pm 0.090$ | 0.010 (rms)        | 0.010 (rms)        |
| 0   | 90.5       | $< 0.516$         | —                            | $16.171 \pm 0.106$ | 0.020 (rms)        | 0.020 (rms)        |
| 1   | 92.4       | $< 0.516$         | —                            | $16.054 \pm 0.110$ | 0.019 (rms)        | 0.019 (rms)        |
| 2   | 102.5      | $< 0.519$         | —                            | $15.370 \pm 0.113$ | 0.019 (rms)        | 0.019 (rms)        |
| 3   | 104.5      | $< 0.535$         | —                            | $15.206 \pm 0.111$ | 0.019 (rms)        | 0.019 (rms)        |

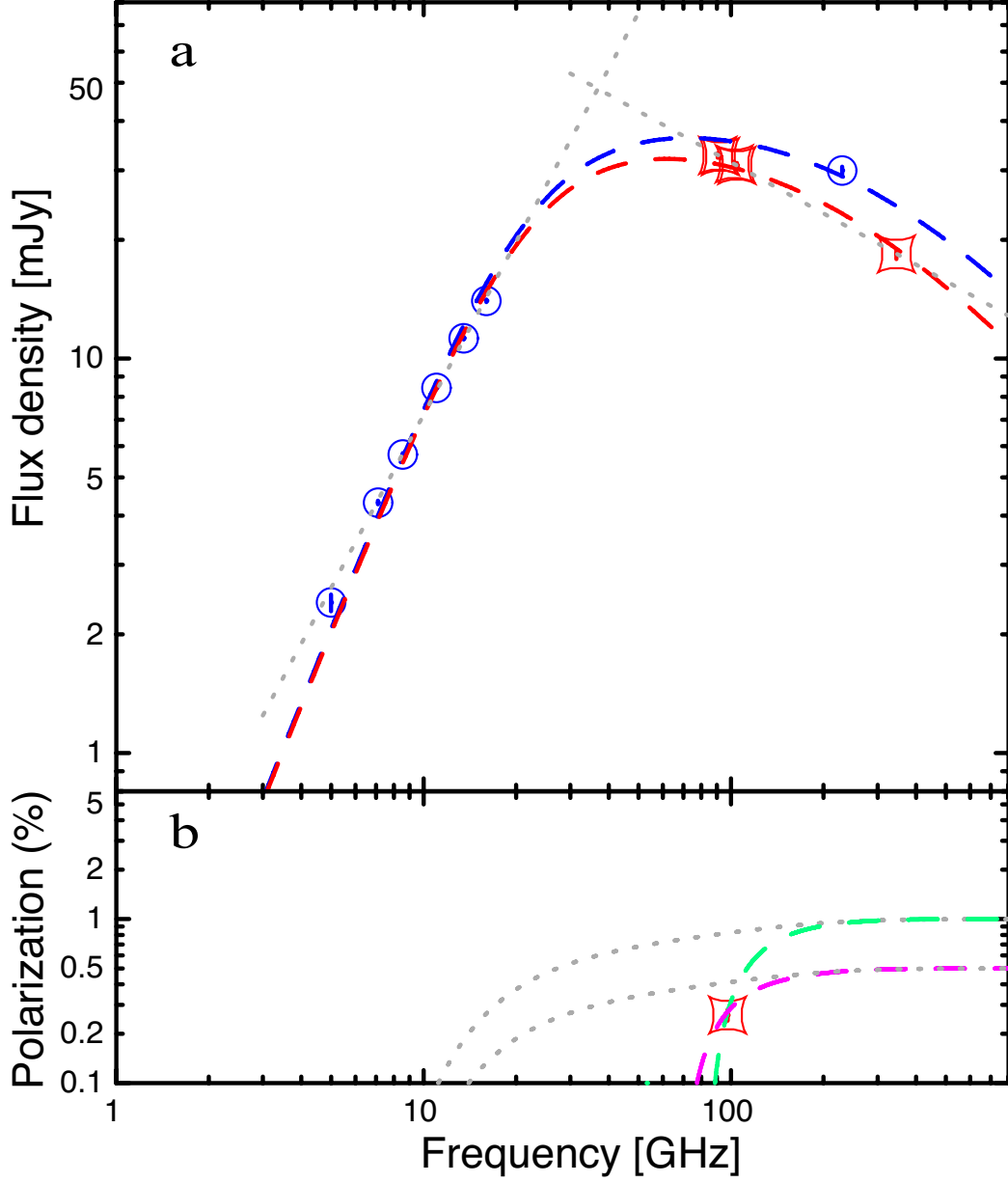


**Figure 2.** Spectral flux distributions and polarization spectrum of the GRB 171205A afterglow. a, Spectral flux distribution at 4.1 days (blue circles and model dashed line) and 5.2 days (red squared points and model dashed line) after burst. The grey dotted lines indicate the simple power-law functions with index of 1.457 and -0.430. b, Polarization spectrum with the ALMA measurement 5.2 days after the burst. Dashed lines indicate the Faraday depolarized spectrum by assuming  $P_0$  of 1% (green) and 0.5% (magenta). The grey dotted lines indicate the polarization spectrum without the Faraday depolarization effect (i.e. all electrons are energized by the relativistic shock).

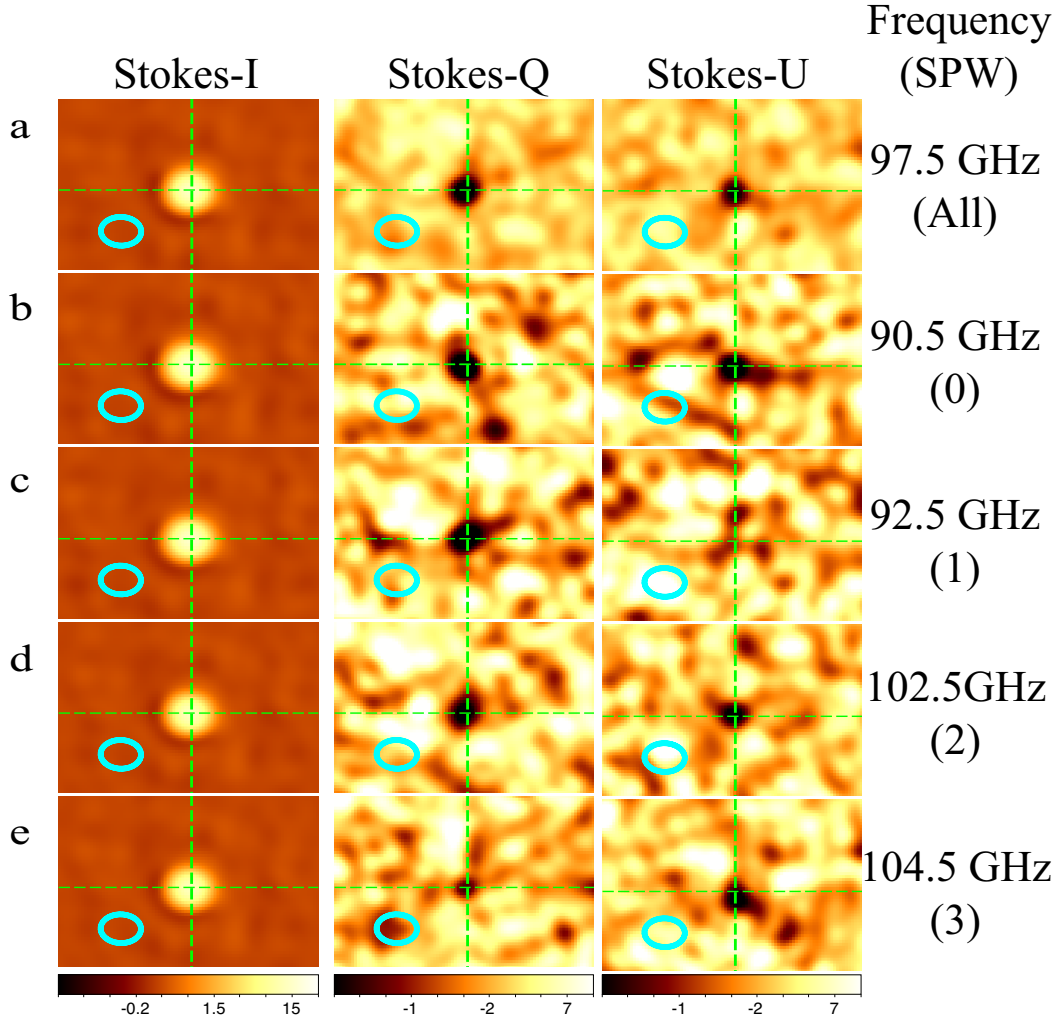


**Figure 3.** The Stokes  $I$ ,  $Q$ , and  $U$  maps ( $5'' \times 3''$ ) of the afterglow of GRB 171205A taken on 10 December 2018 (5.187 days after the burst). The ALMA beam size is shown with the open cyan circles. The map created using the entire ALMA Band 3 dataset with a representative frequency of 97.5 GHz (a), and four individual spectral windows (SPW) with a representative frequency of 90.5 GHz (b), 92.5 GHz (c), 102.5 GHz (d), and 104.5 GHz (e). The units of color bars are mJy for Stokes  $I$  and  $\mu\text{Jy}$  for Stokes  $Q$  and  $U$  maps.



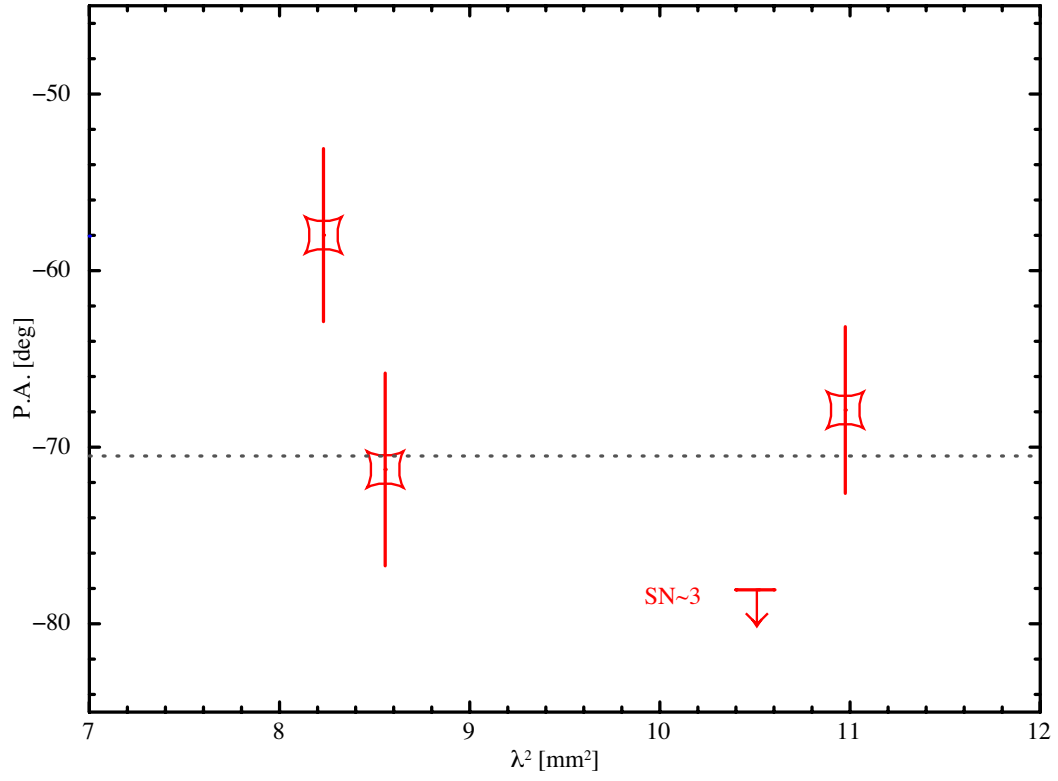


**Figure 4.** The position angle (P.A.) of the GRB171205A afterglow as a function of wavelength. Squared points indicate the observed P.A. at 90.5, 102.5, 104.5 GHz. The upper limit at 92.5 GHz with a signal-to-noise ratio of 3 is also plotted with a red arrow. The grey dotted line indicates the constant fitting function with a reduced chi-square of 4.5 (d.o.f = 3).